Environmental Science and Pollution Research (2020) 27:39317–39329
https://doi.org/10.1007/s11356-020-10004-x

RESEARCH ARTICLE

Chemical footprints of harmattan dust and traffic corridor particulates monitored at two environmentally distinct geopolitical zones in Nigeria

Olawale E. Abiye[1] · Olaniran J. Matthew[2] · Akeem B. Rabiu[3] · Godwin C. Ezeh[1] · Oluseyi E. Akinola[4] · Gunchin Gerelmaa[5] · Chinonso E. Ugwumadu[1] · Moufthou B. Latif[1]

Received: 21 March 2020 / Accepted: 2 July 2020 / Published online: 9 July 2020

Abstract

Harmattan dust and traffic-related pollution have been a serious environmental concern in the West African sub-region. In order to further contribute to the understanding of ambient levels of atmospheric pollution and chemical composition in the region, this study monitored harmattan dust and traffic-related particulate matter at four locations across southwestern (Ile-Ife) and northwestern (Zaria) geo-political zones of Nigeria. The collected samples were characterized for their chemical composition using Energy-Dispersive X-Ray Fluorescence spectrometer equipped with an optimized secondary target x-ray excitation conditions (Al, CaF_2, Fe, Ge, Zr, Mo, Ag, Al_2O_3). The objectives are to assess spatio-temporal mass concentrations, chemical footprints, enrichment factors, elemental correlations, and ratios at all locations. The X-ray analytical method was validated with a NIST SRM 2783 air particulate standard, and detection limits for each chemical specie were determined. Validation results showed good reproducibility of the certified reference material with relative standard deviations of the elements much lower by about 1–13% than the corresponding reference values. Mass concentrations reached up to 2200 μgm^{-3} in the north and 1500 μgm^{-3} in the south. The range of mean concentration of crustal marker elements were Al (5–27 μgm^{-3}), Si (5–856 μgm^{-3}), Ca (0.78–13 μgm^{-3}), and Fe (2–13 μgm^{-3}), and were most abundant during the harmattan particularly in the southwestern region. Highest mean concentration values of 380, 810, and 420 ngm^{-3} were recorded for Cr, Cu, and Pb respectively at the traffic corridor which also recorded the highest enrichment factors. Black carbon and elemental concentrations contributed between 1 to 54% and 9 to 94% across the locations respectively. Backward trajectories of atmospheric flow over the locations showed two dominant sources; dust laden source from the Sahara desert and maritime flow over the Gulf of Guinea. This study found that chemical footprints (Al, Si, K, Ca, Ti, and Fe) of harmattan-related dust were more correlated (r^2 between 0.88 and 0.99) than those attributed to dust re-suspension at the traffic location.

Keywords Particulates · XRF · Detection limits · Traffic · HYSPLIT · Uncertainty

Responsible Editor: Gerhard Lammel

✉ Olawale E. Abiye
waleabiye@gmail.com

[1] Centre for Energy Research and Development, Obafemi Awolowo University, Ile-Ife, Nigeria

[2] Institute of Ecology and Environmental Studies, Obafemi Awolowo University, Ile-Ife, Nigeria

[3] Centre for Atmospheric Research, Kogi State University Campus, Anyigba, Nigeria

[4] Department of Physics and Engineering Physics, Obafemi Awolowo University, Ile-Ife, Nigeria

[5] Vienna University of Technology Atominstitut, Vienna, Austria

Introduction

Among the nine regions (the Arabian Peninsula, Central Asia, North African Sahara, South Africa, Western China, Eastern China, North America, South America, and Australia) identified as contributors to total global production of desert dust (Prospero et al. 2002; Tanaka and Chiba 2006), the Sahara desert has been unequivocally spotted as a major source (Engelstaedter et al. 2006; De Longueville et al. 2010). It has been estimated that almost 1100 Tg $year^{-1}$ (roughly 58%) of total global dust emission comes from the Sahara desert (Tanaka and Chiba 2006). Excluding the transport over the African continent itself, the atmospheric trajectories of dust-laden air masses from the Sahara desert are categorized

into three. Namely, transport across the Atlantic Ocean to North and South America, transport to Mediterranean and Europe, and transport to Eastern Mediterranean and Middle East; each occurring at specific time of the year with varying inter-annual intensities (Anuforom 2007). Though earlier study (D'Almeida 1989) has shown that 60% of particles from the Saharan desert are transported by north-easterly trade wind in a south-westerly direction to the Gulf of Guinea, less attention has been given to the physical and chemical characterization of desert dust over the region (Adedokun et al. 1989) until recently (e.g., Resch et al. 2008 and Sunnu et al. 2008 in Ghana, McTainsh et al. 1997 in Mali and Anuforom 2007 in Nigeria).

The transport of Saharan dust episode (Chiapello 2014; Shao et al. 2011) and its weather modification typically called harmattan is ranked topmost natural process contributing to air quality deterioration in Sub-Saharan Africa. Traffic, vehicular and tail-pipe, and industrial pollution on the other hand are major anthropogenic sources (Mari et al. 2011). In eastern Mediterranean for instance, 50% of days with PM levels higher than the set EU limits have been attributed to Saharan dust occurrence with varied influence within urban and background locations (Kallos et al. 2007; Astitha et al. 2008; Contini et al. 2014). In Africa, harmattan which characteristically occurs between November of a particular year and March of the following year in the West African sub-region is marked with Northerly/North Easterly wind regime that has a long trajectory over the Sahara desert, thus becoming dry and dust-ladden (Adedayo 1980; Adedokun et al. 1989). On the other hand, traffic emission is a major driver of air quality degradation in the region due to factors such as rapid population growth and urbanization, excessively emissions from vehicular fleet that are old and poorly maintained, low grade gasoline combustion and increasing influx, and use of two-stroke engines for transportation purposes as well as use of electric generators (Assamoi and Liousse 2010; Liousse et al. 2014). Globally, exposure to particulate matter (PM) from Saharan dust and traffic pollution have been implicated to have severe effects on human and environmental health (Brauer et al. 2002; Bollati et al. 2010; Rissler et al. 2012) and adverse biometeorological conditions (Nastos et al. 2016; Athanasopoulou et al. 2016). Also, it has also been implicated to cause reversals in atmospheric potential gradient (Ette 1971), poor visibility (Masri et al. 2017), and enhancement of long-range transboundary transport of bio-particulates and disease-causing pathogens (Polymenakou et al. 2008; Gonzalez-Martin et al. 2014).

Previously in Nigeria, Asubiojo et al. (1993) had reported on the chemical constituents of harmattan dust monitored in 1988/89 at two separate cities; Kano and Ile-Ife. Fawole et al. (2016) studied the composition, morphology, and air mass trajectory for identifying possible sources of size-segregated particulates monitored at Ile-Ife during the episode of year 2010. While the study by Fawole et al. (2016) was temporally and spatially limited in terms of sampling days and measurement locations, Asubiojo et al. (1993) could not support attributed sources with trajectory analysis. Other similar studies (Falaiye et al. 2013; Falaiye and Aweda 2018) in the country focused mainly on the characterization of dry depositions of harmattan dust rather than ambient particulates. In this study, we extend the scope of previous studies by improving on the measurement timescale and location characteristics. The study also applied a highly sensitive X-ray fluorescence analytical method. The goal is to compare gravimetric and chemical composition within this period and assess the contributions from possible sources.

Material and methods

Site description

Four measurement locations with different site characteristics (residential, academic, traffic, and background) situated across two environmentally distinct geographic zones were used in this study. The city of Ile-Ife in Osun state and Zaria in Kaduna state of Nigeria were used in this study (Fig. 1). Typical of the West Africa region, Nigeria is characterized by a south-north vegetation gradient and weather variation (Omotosho and Abiodun 2007; Ogungbenro and Morakinyo 2014; Knippertz et al. 2017). Ile-Ife in the southwest is situated within the rain forest vegetation zone while Zaria in the north-west is in the Sudan Savannah. Marked with two main seasons, rainy and dry, annual rainfall follows a mono-modal pattern in the north as against bi-modal in the south of Nigeria. Compared to Ile-Ife, Zaria has more prolonged dry season with average annual rainfall of about 700 mm; a value less by 600 mm to records in Ile-Ife. Particulate matter measurement was carried out in four phases: (i) 6th–31st January, 2016 on the roof top of Physics and Engineering Physics building (7° 31′ 10.3″ N, 4° 31′ 15.4″ E, 294 m asl) in Obafemi Awolowo University, Ile-Ife; (ii) 11th January–29th April, 2017 (11° 09′ 12.8″ N, 7° 39′ 21.0″ E) within the Kongo campus of Ahmadu Bello University, Zaria; (iii) 20th October–13th November, 2017 at Lagere (7° 29′ 15.8″ N, 4° 32′ 38.0″ E) which is a section of a busy road traversing the ancient city of Ile-Ife; and (iv) 11th–28th January, 2018 at the roof top (7° 30′ 24.6″ N, 4° 31′ 16.2″ E) of Atmospheric Research and Information Analysis laboratory, Centre for Energy Research and Development, Obafemi Awolowo University, Ile-Ife. Phases (i), (ii), and (iv) PM samples were collected during Saharan dust occurrence. Hereafter, phase (i) is referred to as RF2016 (i.e., sampling at Rain Forest (RF) location in 2016), phase (ii) as AR2017 (i.e., sampling at Arid (AR) location in 2017), phase (iii) as TRF2017 (i.e., sampling at Traffic (TRF) location in 2017), and phase (iv) as RF2018 following the initial nomenclature.

Fig. 1 Maps showing monitoring locations in **a** the two geopolitical locations **b** a section of Obafemi Awolowo University for RF2016 and RF2018, **c** a section of Ile-Ife town for TRF2017, and **d** a section of Kongo Campus, Ahmadu Bello University, Zaria for AR2017

Sampling

A single port modified version from the ISO 9835:1993 8-port UK sampler was deployed for daily measurement between 08:00 and 20:00 GMT +1. However, the sampling days were not sequential due to power supply outages but it was ensured that the duration for each valid sample collected was essentially the same. It is a low volume sampler equipped with a dry gas meter readable to 0.01 m^3, and accurate to ± 3% at a flow rate of approximately 2 m^3 per day. The collecting funnel at the end of the tube linked to the sampler manifold was suspended at height 2.5 m facing the prevailing wind direction. Captured total suspended particulate matter was deposited on Whatman polycarbonate nuclepore (1.5 μm pore size; 47 mm diameter) filter membranes. Filters used were pre-weighed using Sartorius Microbalance with sensitivity of 0.001 mg. The microweighing balance was calibrated using automated isoCAL function. Mass balance analysis of each post field sample was taken in triplicates and pre-conditioned to a constant humidity and temperature in a desiccator before chemical analysis via x-ray fluorescence technique.

Black carbon measurement

Triplicate measurement of the filters was made using a Smoke Stain reflectometer (m43D) based on reflectance method (Begum et al. 2004; Kothai et al. 2011). From the reflectance R, black carbon concentration C in μgm^{-3} were calculated following the British Standard smoke calibration curve (BS 1747: Part 2: 1991) as follows;

$$C = F/V(91679.22{-}3.332.0460R + 49.6189R^2{-}0.3533R^3 + 0.001R^4)\ for\ 40{\le}R{\le}70$$

$$C = F/V(214245.1{-}15130.512R + 508.181R^2{-}8.831R^3 + 0.0628R^4)\ for\ 40 > R > 10$$

where F is a factor relating to clamp size and has an assigned value of 12.8 in this case.

XRF chemical characterization

The samples were characterized for their chemical compositions using PANanalytical Epsilon 5 energy dispersive x-ray (ED-XRF) spectrometer hosted at the IAEA's Nuclear

Table 1 Secondary targets, detectable elements, and operating conditions of the Epsilon 5 XRF analyzer

*Secondary target	Detectable elements	Voltage (kV)	Current (mA)
Al	Na, Mg	25	24
CaF_2	Al, Si, P, S, Cl, K	40	15
Fe	Ca, Sc, Ti, V, Cr	75	8
Ge	Mn, Fe, Co, Ni, Cu, Zn	75	8
Zr	Ga, Ge, As, Se, Br	100	6
Mo	Sr, Y	100	6
Ag	Zr, Nb, Mo, Tc, Ru	100	6
Al_2O_3	Rh, Pd, Ag, Cd, In, Sn, Sb, Te, I, Cs, Ba, La, Ce	100	6

*Each condition was measured for 300 s

Science and Instrumentation Analysis Laboratory (NSIL), Seibersdorf, Austria. The Epsilon 5 is a fully integrated analyzer with optimized three-dimensional polarizing geometry. Equipped with a W/Sc X-ray tube, it operates at a maximum power of 600 W between voltages 25 and 100 kV. The high energy makes it capable of exciting K-line x-ray of heavy elements such as cadmium. Using a set of programmable polarization and up to 15 secondary targets, the spectrometer can be tuned to get the lowest possible detection limits for most elements in the periodic table. The Epsilon 5 was set up with eight secondary targets (Al, CaF2, Fe, Ge, Zr, Mo, Ag, Al_2O_3) and more than twenty-three calibration curves. Operational conditions for each secondary excitation are presented in Table 1.

Uncertainty estimates

The uncertainty estimates were based on three fundamental parameters namely those arising from (i) peak area (P_{unc}), (ii) X-ray attenuation (A_{unc}), and (iii) calibration(C_{unc}). Actual elemental peak intensity was obtained from the sensitivity by normalizing to time and the current for each

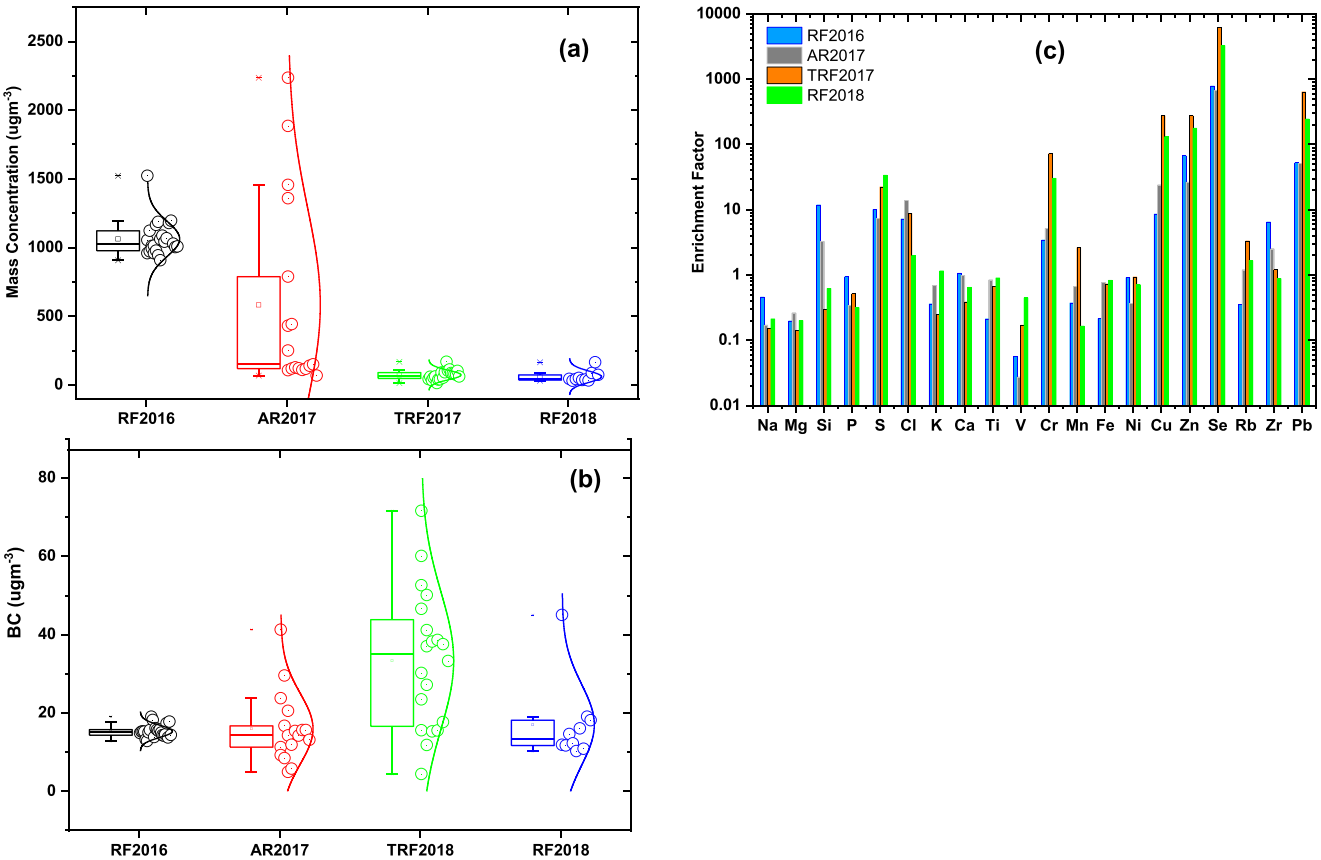

Fig. 2 Distribution of **a** mass concentration, **b** black carbon, and **c** enrichment factor at each location

Table 2 Method detection limits (MDL) and quality control results ($ngcm^{-2}$)

Element	MDL	Method validation (NIST SRM 2783)	
		This study	Certified value
Na	79.2	282 ± 12 (5)*	187 ± 11 (6)*
Mg	31.4	614 ± 17 (3)	866 ± 53 (7)
Al	117.2	2225 ± 6 (1)	2331 ± 54 (3)
Si	656.9	5205 ± 21 (1)	5884 ± 161 (3)
K	68.7	509 ± 1 (1)	531 ± 57 (11)
Ca	41.4	1163 ± 26 (3)	1326 ± 171 (13)
Ti	3.8	143 ± 6 (4)	150 ± 25 (17)
Cr	2.9	13 ± 3 (19)	14 ± 3 (19)
Mn	3.6	32 ± 1 (2)	33 ± 2 (4)
Fe	14.5	2596 ± 1 (1)	2661 ± 161 (7)
Ni	1.5	7 ± 1 (6)	7 ± 2 (18)
Cu	4.2	38 ± 3 (7)	41 ± 5 (11)
Zn	3.2	180 ± 3 (2)	180 ± 14 (8)
Pb	7.5	35 ± 4 (10)	32 ± 6 (18)

*Values in parenthesis are the relative standard deviation in percentage

secondary excitation condition. For the calibration, we considered both the micromatter standards nominal uncertainties (μ_{unc}) of 5% and fit errors from calibration curves(∞_{unc}). Attenuation uncertainties of 16% for Na, 12% for Mg, 11% for both Al and Si, and 1% for all others were taken from Manousakas et al. (2017) following the proposal of Gutknecht et al. (2010) and applied in this work. Thereafter, combine uncertainty (T_{unc}) for the XRF analytical method applied in this study was estimated for each element i per analyzed filter j as follows

$$T_{\mathrm{unc},\ i;j} = \sqrt{P^2_{\mathrm{unc},\ i;j} + A^2_{\mathrm{unc},i;j} + C^2_{\mathrm{unc},i;j}} \quad (1)$$

where

$$C^2_{\mathrm{unc},i;j} = \mu^2_{\mathrm{unc},i:j} + \infty^2_{\mathrm{unc},i:j} \quad (2)$$

Enrichment factors, elemental ratio, and correlation

Relative contributions from natural and anthropogenic sources to the chemical composition of the collected particulates were examined through enrichment factor (EF) analysis. The EF methodology, regardless of the identified limitation (Reimann and Caritat 2000), has been widely applied as the first indication of source fingerprints (Arditsoglou and Samara 2005; Çevik et al. 2009; Ezeh et al. 2018). It normalizes the concentration

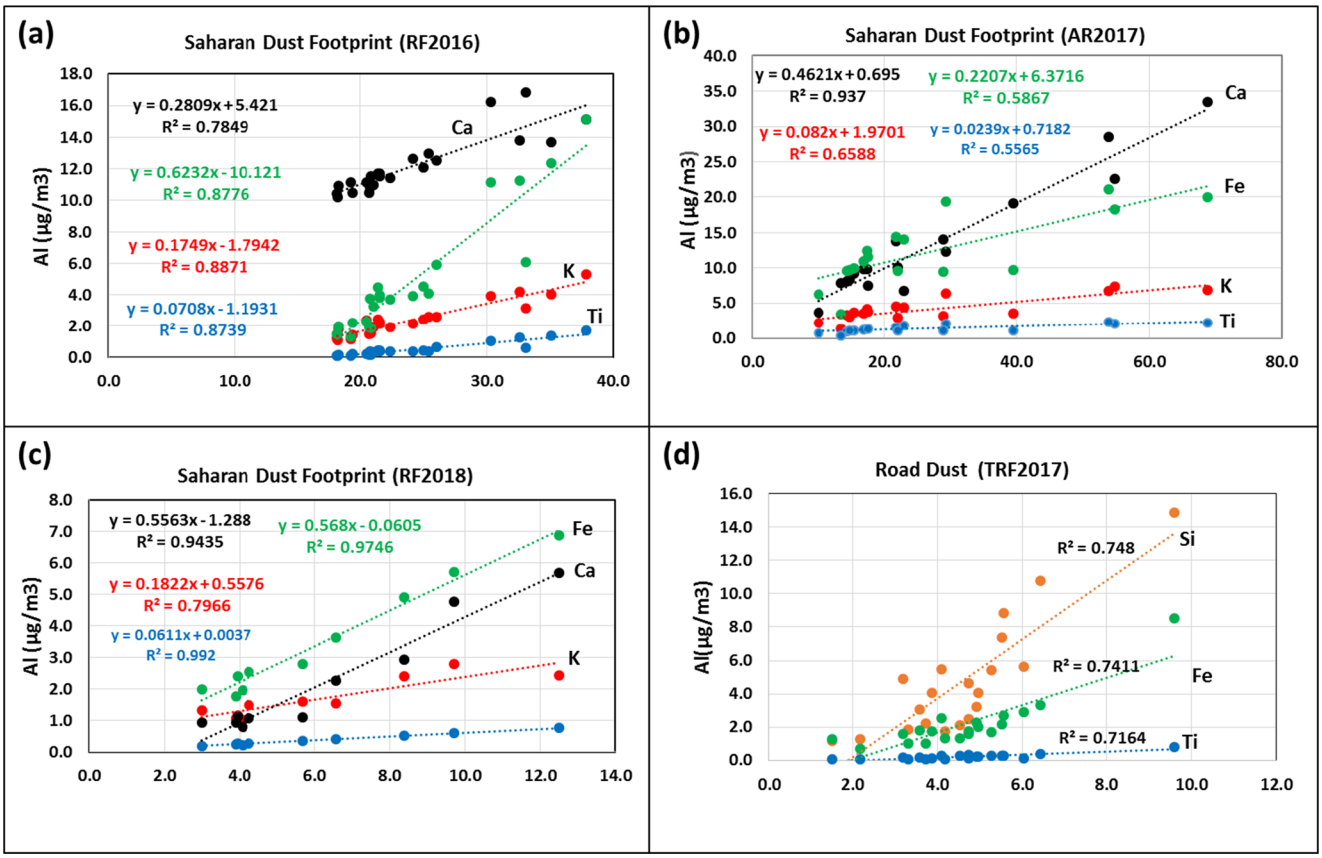

Fig. 3 Correlates of marker elements for Saharan and road dust

of a chemical specie X in a given sample; in this case, the atmospheric particulates monitored to a reference specie (aluminum has been used in this study) that is assumed to have negligible anthropogenic influence in contributing to continental crust. Applying reference values of crustal composition from Mason and Moore (1982), the EF was calculated as follows:

$$\frac{X_{\text{atm}}/\text{Al}_{\text{atm}}}{X_{\text{Crust}}/\text{Al}_{\text{crust}}} \quad (3)$$

where X_{atm} and Al_{atm} are the concentrations of the chemical specie and Al in the TSP respectively. X_{Crust} and Al_{crust} are the respective concentrations in the reference earth crust.

HYSPLIT backtrajectory

To track the air mass transport of TSP to the sampling locations, HYSPLIT model (Draxler and Rolph 2003; Stein et al. 2015) runs of a 5-day backtrajectory analysis were performed through the web-based Real-time Environmental Application and Display sYstem: READY (Rolph et al. 2017). The system provides a quasi-operation portal to remotely run HYSPLIT atmospheric transport and dispersion model with archive or forecast meteorological data (Stein et al. 2015; Rolph et al. 2017). We used Reanalysis data and considered air transport at 3 levels: 500 m, 1000 m, and 1500 m above ground level and representing a combination of near-ground and upper boundary layer (Dimitriou and Kassomenos 2018).

Result and discussion

Mass and elemental concentrations

Mass and elemental concentrations of the PM measured in the Southern locations (RF2016 and RF2018), northern arid location (AR2017), and at the traffic corridor (TRF2018) are presented in Table 3. Also, the estimated uncertainty associated with each analytical results was

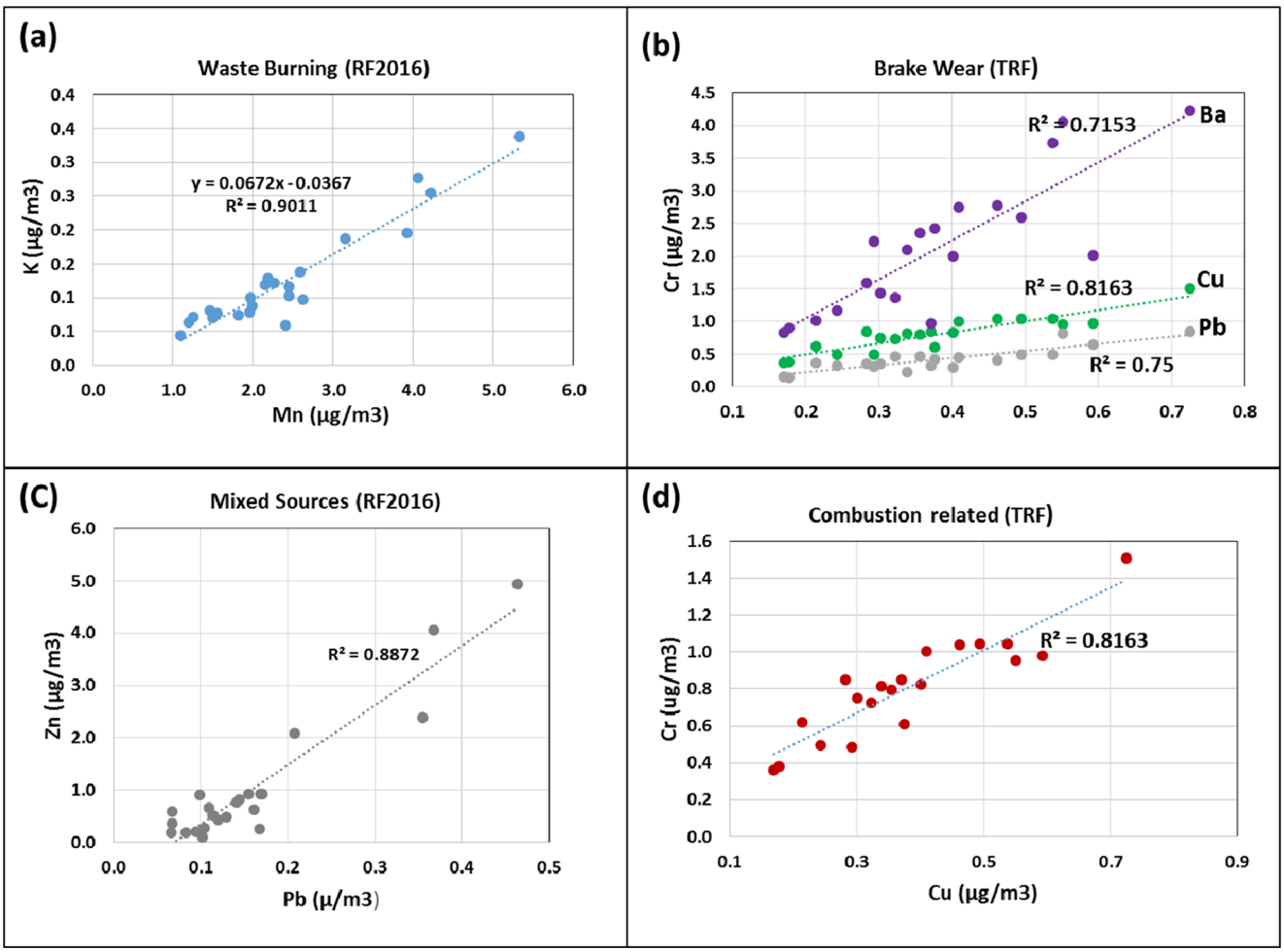

Fig. 4 Correlates of marker elements for other sources

Table 3 Summary of mass and chemical specie concentration per sampling location

	RF2016 (n = 23)		AR2017 (n = 17)		TRF2017 (n = 20)		RF2018 (10)	
	Mean (range) Uncertainty (μgm^{-3})							
TSP	1063 (907–1522)	----	583 (68–2235)	----	73 (14–170)	----	61 (32–166)	–
BC	16 (13–19)	----	16 (5–42)	----	33 (4–72)	----	17 (10–45)	----
Na	3 (2–4)	*0.079*	2 (0.2–5)	*0.038*	0.2 (0.01–0.3)	*0.234*	0.4 (0.2–0.8)	*0.007*
Mg	2 (1–3)	*0.037*	2 (0.3–4)	*0.040*	0.2 (0.2–0.2)	*0.257*	0.4 (0.01–1)	*0.107*
Al	24 (18–40)	*0.422*	27 (10–69)	*0.380*	5 (2–10)	*0.026*	6 (3–13)	*0.059*
Si	856 (710–1234)	*25.62*	414 (17–1688)	*10.61*	5 (1–15)	*0.050*	14 (6–30)	*0.226*
K	5 (1–5)	*0.025*	4.2 (1–7)	*0.033*	0.3 (0.1–1)	*0.002*	2 (1–3)	*0.011*
Ca	12 (10–16)	*0.150*	13 (4–34)	*0.132*	0.78 (0.2–3)	*0.004*	2 (1–6)	*0.014*
Ti	0.5 (0.1–2)	*0.006*	2 (0.4–2.3)	*0.012*	0.3 (0.06–0.8)	*0.001*	0.4 (0.2–0.8)	*0.003*
Fe	5 (2–15)	*0.062*	13 (4–21)	*0.118*	2 (0.7–9)	*0.009*	4 (2–7)	*0.024*
	Mean (range) Uncertainty (ngm^{-3})							
P	260 (180–440)	----	140 (10–500)	----	300 (100–800)	----	20 (10–30)	----
S	650 (100–1270)	*6.72*	560 (230–1130)	*4.76*	190 (100–510)	*7.18*	500 (10–910)	*5.93*
Cl	280 (50–740)	*5.77*	530 (80–1140)	*8.52*	500 (100–940)	*10.9*	30 (10–0.200)	*8.39*
V	10 (1–20)	–	10 (1–10)		nd	----	10 (1–20)	----
Cr	90 (70–110)	*0.96*	130 (40–220)	*1.02*	380 (170–720)	*1.18*	210 (70–460)	*1.13*
Mn	130 (40–340)	*1.96*	200 (040–0.46)	*2.55*	700 (200–500)	*4.46*	10 (10–30)	*12.3*
Ni	20 (0–40)	*0.24*	10 (1–30)	*2.65*	nd	----	10 (2–12)	----
Cu	130 (90–290)	*1.42*	310 (50–630)	*2.24*	810 (360–1510)	*2.50*	510 (180–1140)	*2.71*
Zn	1030 (110–4930)	*13.44*	620 (60–4820)	*5.45*	810 (460–1930)	*3.52*	780 (440–1530)	*6.80*
Ga	140 (110–200)	*1.61*	330 (60–650)	*2.54*	1040 (430–1900)	*3.22*	580 (190–1250)	*3.16*
As	40 (1–90)	*0.56*	60 (1–130)	*0.56*	160 (70–280)	*0.62*	100 (40–210)	*0.68*
Se	10 [1–20]	----	10 (1–30)	----	20 (10–80)	----	10 (2–20)	*14.6*
Rb	10 [1–30]	----	30 (1–70)	----	10 (5–60)	----	10 (5–40)	----
Zr	290 (240–410)	*3.09*	180 (10–62)	*1.66*	10 (4–30)	*12.0*	10 (2–20)	*7.61*
Ba	440 (270–600)	*5.30*	870 (270–1380)	*7.34*	2130 (820–4230)	*7.04*	1460 (360–4110)	*7.95*
Pb	160 (70–460)	*2.17*	180 (50–480)	*1.77*	420 (130–850)	*1.70*	220 (70–460)	*1.58*

n, number of PM filters analyzed; *nd*, not detected; ——, uncertainty not determined, italicized values are the associated uncertainties

included in Table 3. Comparative distributions of BC to the mass concentrations at each location are presented in Fig. 2a, b. Daily values reached up to 2200 μgm^{-3} in the arid zone and 1500 μgm^{-3} in the rainforest. However, the mean TSP values were highest in the rainforest location (1063 μgm^{-3}) than in arid (583 μgm^{-3}) region probably due to the extension of measurement beyond the harmattan period. Although the mass concentrations were much higher than those reported by previous and similar studies in Nigeria (up to 1033 μgm^{-3} in Kano and 329 μgm^{-3} in Ile-Ife for TSP by Asubiojo et al. 1993; 400 μgm^{-3} for PM_{10} by Fawole et al. 2016; 780 μgm^{-3} in Ile-Ife for TSP by Abiye et al. 2019), it proves the case that dust intensities varies by season, year, and the geographic location (Anuforom 2007). The implication of this result is that harmattan dust needs to be continuously measured to understand the atmospheric dynamics influencing ground concentrations of PM. The quality control and the detection limits data for the XRF analytical method are shown in Table 2. The values obtained showed a good reproducibility of the reference materials by the analytical method. Crustal markers elements (Al, Si, Ca) were most dominant during the SDE's but more higher in the RF2016 episode. While Al, Si, and Ca are 5 to 172 times higher than their corresponding values at the TRF, BC [33 μgm^{-3}], Mn [700 ngm^{-3}], and Pb [420 ngm^{-3}] at the traffic corridor were at least double the values obtained during the SDE's. BC and elemental species contributed between 1 to 2% and 82 to 87% at RF2016, 1 to 23% and 54 to 94% at AR2017, 22 to 40% and 41 to 65% at RF2018 while at the traffic corridor, the contributions were 20 to 54% and 9 to 70% respectively to the TSP loadings. Mean concentration of Se [10 ng^{-3}] was the same for the all three SDE locations but twice the value [20 ngm^{-3}] at the traffic location. Sulfur concentration was almost the same [570 ngm^{-3}] across the SDE locations but much lesser [190 ngm^{-3}] at the traffic site. Similar to the results

Table 4 Mean elemental ratios of selected

	Zn/Pb	As/V	V/Ni	Se/S
RF2016	5.4 ± 2.9 (1.0–11.1)	6.1 ± 3.5 (2.0–13.2)	0.5 ± 0.3 (0.2–0.9)	0.02 ± 0.01 (0.006–0.032)
AR2017	2.7 ± 2.0 (0.9–10)	8.4 ± 7.2 (0.3–14.0)	1.0 ± 0.9 (0.2–2.2)	0.02 ± 0.01 (0.001–0.04)
TRF2017	2.2 ± 1.2 (1.0–6.4)	–	–	0.8 ± 1.5 (0.008–6.03)
RF2018	4.6 ± 4.4 (1.8–16.5)	45.3 ± 64.8 (6.0–141.4)	2.6 ± 2.4 (0.5–5.3)	0.09 ± 0.2 (0.004–0.69)

obtained in Lagos by Ezeh et al. (2018), average concentration of Ni did not exceed the European guideline of 20 ngm^{-3} (WHO 2016) at any of the sites. However, Pb was 3 to 8 times higher than the set limit of 50 ngm^{-3} (WHO 2006). Although the importation of leaded gasoline has been banned in the country, the results here show that traffic (420 ngm^{3}) corridors are still subjected to high exposures of Pb. Considering the ban of leaded gasoline, this trend can be explained in terms of non-combustion vehicular emissions from brake wear (Pant and Harrison 2013). Relative contributions of BC and other identified sources are presented in Fig. 2. Potassium was excluded in the estimate for Saharan dust following Greilinger et al. (2019) since it is known that wood burning is a major contributor to its concentration in PM (Caseiro et al. 2009) and has been identified (Fig. 4a) as emanating from waste burning. Fawole et al. (2016) have shown that mineral dust (SiO2) contributed ~42%, and alumino-silicate accounted for >90% of elemental concentration of Saharan dust episode. Saharan dust is mainly made up of clay minerals, quartz, calcium, and magnesium carbonates compared with particles of anthropogenic origin which have been shown to be made up of a wide composition of other metals (Afeti and Resch 2000; Rodriguez et al. 2001).

Enrichments factors, elemental ratios, and correlations

Elemental ratios ER of selected elements were determined and compared with reported values in literature together with source attributions. ER have been used to estimate source profile, air mass origin, and local source fingerprint (Arditsoglou and Samara 2005). Also, linear correlation was used to provide insight on same source contribution. Average values of EF (Fig. 2c) showed that Si, S, Cl, Cr, Mn, Cu, Zn, Se, Zr, and Pb have significant enrichment across the three locations. Si was enriched up to 9 and 15 times above what is expected in a crustal sample at the AR and RF sites. The EF's are such that Se > Zn > Pb > Si > S > Cu > Zr > Cr during RF2016, Se > Pb > Zn > Cu > S > Cr > Si > Zr during AR2017, Se > Pb > Zn > Cu > Cr > S > Rb > Zr during TRF 2017, and Se > Pb > Zn > Cu > S > Cr > Rb > K during RF2018. Interestingly, Se which is a tracer element for charcoal burning (Watson et al. 2001; Arditsoglou and Samara 2005) has the highest enrichment at all locations. This could possibly be linked to the utilization of charcoal for domestic and small scale commercial heating (Liousse et al. 2014) which is characteristic of residential areas within 1.5 km of the sampling locations. The traffic corridor has the highest EF for Cr (18-110), Cu (97-373), Zn (116-785), Pb (235-1176), and Mn (≤24). These elements have been mainly used as markers for vehicular emissions (Almeida et al. 2006; Crawford et al. 2007; Dongarra et al. 2009; Amato et al. 2011; Pant and Harrison 2013). Typically, EF values approaching unity are footprints indicating the predominance of earth crust pollution sources. EF's > 5 are suggestive of significant portion of the chemical specie being contributed from non-crustal sources (Gao et al. 2002; Arditsoglou and Samara 2005). More so, the higher the EF values, the more contribution is suggested from the suspected sources. Correlates of crustal marker elements (Al, K, Ca, Ti, Fe) associated with the Saharan dust episode are presented in Fig. 3a–c). High correlation of Cr with Ba (0.72), Cu (0.82),

Table 5 Mean (range) of enrichment factors for elemental specie at the locations

	RF2016	AR2017	TRF2017	RF2018
Na	0.41 (0.21–0.65)	0.17 (0.06–0.32)	0.14 (0.01–0.38)	0.21 (0.08–0.33)
Mg	0.2 (0.16–0.24)	0.26 (0.09–0.44)	0.14 (0.06–0.36)	0.18 (0.01–0.33)
Si	10.9 (5.64–14.39)	3.24 (0.49–8.62)	0.28 (0.12–0.49)	0.62 (0.42–0.76)
P	0.88 (0.48–1.2)	0.34 (0.04–0.99)	0.48 (0.1–1.54)	0.3 (0.14–0.54)
S	8.87 (1.8–19.1)	7.32 (3.57–11.1)	17.36 (0.67–102.66)	33.74 (0.99–69.41)
Cl	7.2 (1.43–21.7)	13.71 (3.81–26.67)	6.85 (0.47–107.19)	1.87 (0.46–9.95)
K	0.38 (0.24–0.55)	0.69 (0.35–0.96)	0.22 (0–0.67)	1.14 (0.77–1.76)
Ca	1.02 (0.77–1.18)	0.99 (0.58–1.26)	0.35 (0.07–1.11)	0.62 (0.39–0.97)
Ti	0.27 (0.1–0.66)	0.83 (0.38–1.14)	0.64 (0.24–1.21)	0.89 (0.78–1.01)
V	0.07 (0–0.35)	0.03 (0–0.2)	0.13 (0–2.53)	0.4 (0–2.67)
Cr	3.19 (1.85–4.66)	5.15 (1.78–10.75)	73.4 (18.38–110.94)	29.99 (12.43–57.04)
Mn	0.42 (0.21–0.77)	0.65 (0.37–0.98)	2.16 (0.01–23.91)	0.16 (0.06–0.3)
Fe	0.27 (0.1–0.58)	0.76 (0.36–1.05)	0.66 (0.4–1.3)	0.82 (0.67–0.97)
Ni	0.84 (0.43–2.09)	0.36 (0.01–1)	0.91 (0.37–2.38)	0.7 (0.29–1.2)
Cu	8.33 (4.69–11.51)	23.84 (4.03–56.03)	277.57 (96.65–373.62)	132.01 (55.92–215.27)
Zn	54.72 (6.3–269.49)	26.3 (4.79–103.4)	241.57 (116.51–784.45)	175.13 (69.76–466.08)
Se	670.9 (117–1356)	674.5 (67.96–1347.75)	6978.78 (229.73–25,526.3)	3196.24 (228.7–6434.64)
Rb	0.44 (0–1.56)	1.19 (0–2.8)	3.72 (0–23.99)	1.93 (0–6.33)
Zr	6.12 (4.03–8.49)	2.49 (0.33–5.77)	1.11 (0.05–3.05)	0.87 (0.09–1.64)
Pb	46.35 (12.51–141.88)	50.58 (15.45–93.57)	632.74 (235.79–1176.57)	247.29 (142.39–434.63)

and Pb (0.75) at TRF (Fig. 4b) could be indicative of non-exhaust emission from vehicle abrasion. Specifically, the elements Cr, Ba, Cu, and Pb are typical markers that have been established as footprints for brake wear (Adachi and Tainosho 2004; Wahlin et al. 2006; Song and Gao 2011; Pant and Harrison 2013). The brake wear footprint was distinguished from tyre wear using the proportion of Zn to Cu and Ba. Apeagyei et al. (2011) have shown that the proportion of Zn is about 15 times more in tyre wear than brakes while Cu and Ba are higher in brake materials. Concentrations of Cu and Ba in the present study were nearly 5 times higher than Zn. Also, the average Zn/Pb ratio of 2.2 (Table 3) obtained in this study for the TRF is similar to those reported for light-duty gasoline (1.7) and heavy-duty diesel (1.9) vehicular emissions (Qin et al. 1997; Watson et al. 2001). Correlates of dust-related chemical footprints of Al versus (Si, K, Ca, Ti, and Fe) at the four locations are presented in Fig. 3a–d. The chemicals were better correlated at the RF ($R^2 = 0.80–0.99$) locations than those at the AR (R^2 mostly ~ 0.60 except for Ca [0.94]) during the harmattan period. The weak correlation during AR2017 can be attributed to mixed conditions of both harmattan and non-harmattan period as the measurement spanned from January to April. Interestingly, the correlations of the elements at the traffic corridors were almost the same (~ 0.74) and can be attributed to re-suspended road dust as marker elements for road dust at traffic corridors (Peltier et al. 2011; Harrison et al. 2012). (Tables 4 and 5).

Air mass trajectories during phases of sampling

Backward trajectories of atmospheric flow over the locations show two dominant sources: dust-laden source from the Sahara desert and maritime flow over the Gulf of Guinea. However, the characteristic atmospheric flow varies slightly

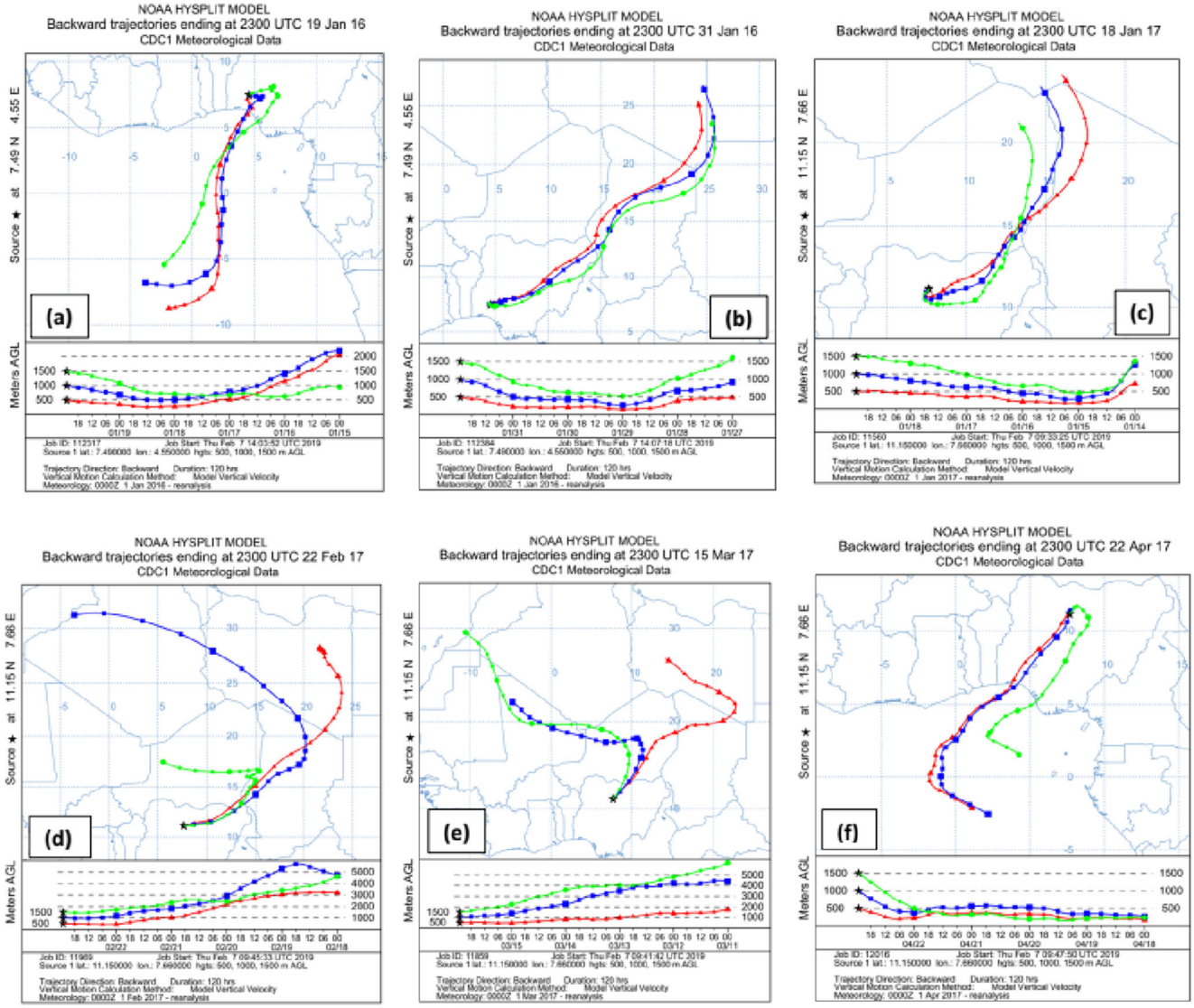

Fig. 5 Five days air mass trajectories arriving at the locations during sampling of phase (i) (**a**, **b**) and phase (ii) (**c**–**f**)

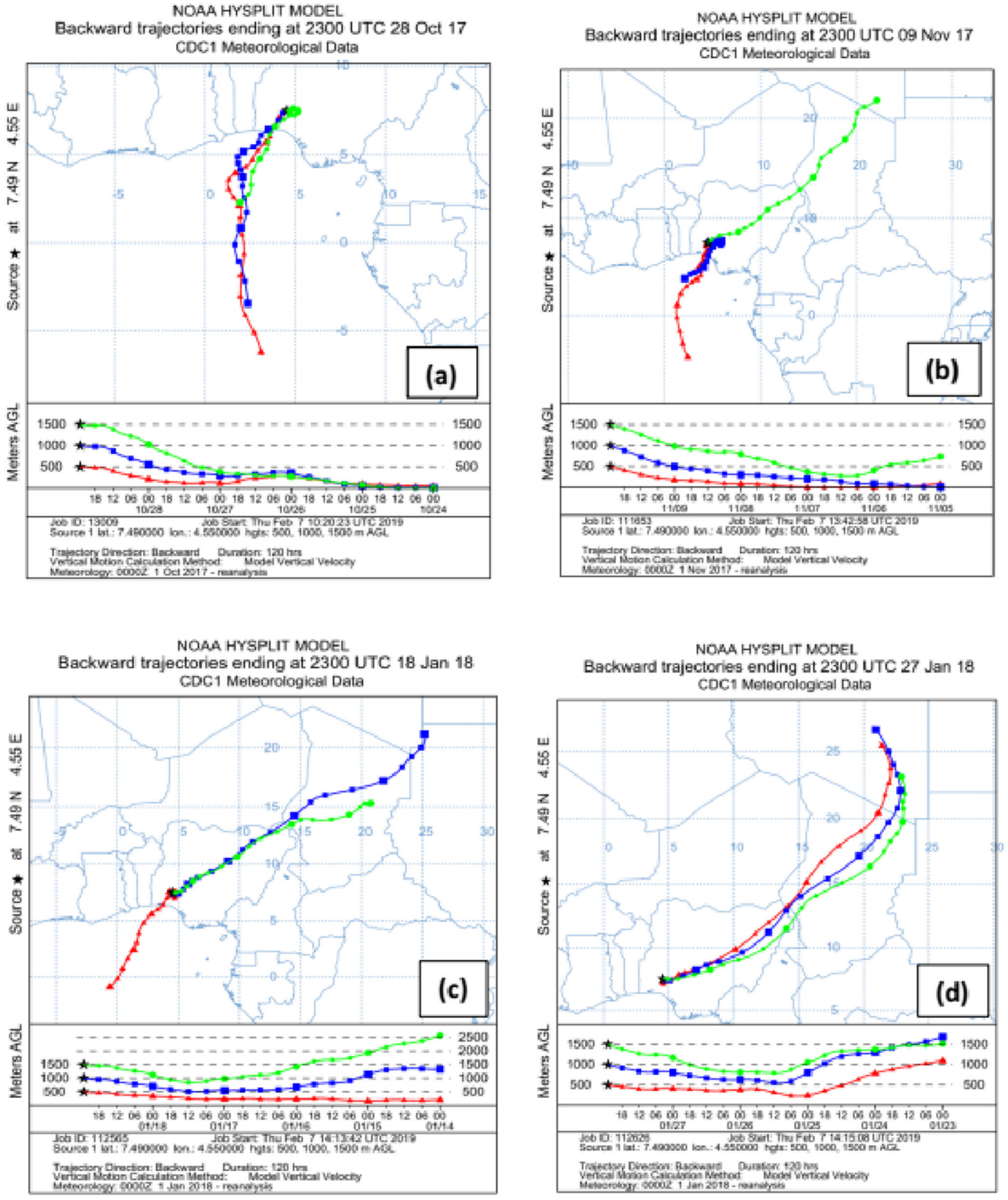

Fig. 6 Five days of air mass trajectories arriving at the locations during sampling of phase (iii) (**a**, **b**) and phase (iv) (**c**, **d**)

during each phase of the particulate sampling and are briefly summarized; Phase (i) 6th–31st January, 2016: Predominant flow at all levels (Fig. 5a, b) were either from the northern Sahara or of maritime origin. While the air masses transported from the northern Sahara to the location maintained the same altitude as at the origin, the maritime flow arriving the

sampling point at lowest 500 m emanated from 2 km at the origin. Phase (ii) 11th January–29th April, 2017: The Saharan air masses (Figs. 5d–f) impacting the location can be separated into three. Those arriving from north central Africa, northern, and Western Sahara. For the most part, the vertical trajectories descend from altitudes of about 5 km to arrive the sampling location at heights much below 1 km. Observed maritime air masses originate from about 500 m but are vented upward to into the upper atmospheric boundary layer. Phase (iii) 20th October–13th November, 2017: The air masses in this period have vertical trajectories (Fig. 6a, b) starting from the surface and arriving the location at higher altitudes. The implication is that sampling done at this time is more likely to be influenced by local sources rather than long-range transport of remote sources. Phase (iv) 11th–28th January, 2018: Air mass trajectories (Fig. 6c, d) are quite similar to those in phase (ii) in terms of vertical transport from the source except that less maritime flow was observed. Across the phases, only (i), (ii), and (iv) are significantly impacted by the long-range transport of air mass over the Sahara and thus, the sampling during those period satisfies the objectives.

Conclusion

Energy dispersive XRF spectrometer has been used to analyze chemical contents of harmattan dust and traffic corridor airborne particulates collected at four different sites across two environmentally distinct zones in Nigeria. The XRF analytical method was highly sensitive with very a low detection limit and uncertainties. Chemical footprints (Al, Si, K, Ca, Ti, and Fe) of harmattan-related dust were more correlated than those attributed to re-suspension at the traffic location. Mass concentration of black carbon, Cr, Mn, Ni, Cu, As, and Pb were the highest and most enriched at the traffic corridor. Atmospheric flow from Sahara desert and the Gulf of Guinea were the main sources of impacting on the locations.

Acknowledgments O. E. Abiye and C. E. Ugwumadu are grateful for International Atomic Energy Agency (IAEA) Training Fellowship at the Agency's Nuclear Science and Instrumentation Laboratory (NSIL) in Seibersdorf, Austria. We specially thank Prof. Piet Van Espen of Antwerp University Belgium, Drs. Roman Padilla Avarez and Allessandro Migrioli for their mentorship. O. E. Abiye is grateful for the travel support received from Centre for Atmospheric Research (CAR) Kogi State University Campus, National Space Research and Development Agency, Nigeria to present this work at The Sao Paulo School of Advance Science on Atmospheric Aerosols, Brazil in 2019. The authors gratefully acknowledge the NOAA Air Resources Laboratory (ARL) for the provision of the HYSPLIT transport and dispersion model and READY website (http://www.ready.noaa.gov) used in this publication. The modified 8-port sampler and consumables used in this study were generously donated by Dr. Monica Price of Faculty of Health Sciences & Wellbeing, University of Sunderland, UK and is hereby appreciated.

References

Abiye OE, Price A, Price M (2019) Biogenic and natural components of Saharan dust sampled in Nigeria. Hum Ecol Risk Assess:1–10. https://doi.org/10.1080/10807039.2019.1628635

Adachi K, Tainosho Y (2004) Characterization of heavy metal particles embedded in tire dust. Environ Int 30:1009–1017

Adedayo SI (1980) Pronounced dust haze spell over Nigeria. 2–11 March, In Pre-WAMEX Symposium. Lagos, Nigeria

Adedokun JA, Emofurieta WO, Adedeji OA (1989) Physical, mineralogical and chemical prosperities of harmattan dust at Ile-Ife, Nigeria. Theor Appl Climatol 40:161–169

Afeti GM, Resch FJ (2000) Physical characteristics of Saharan dust near the Gulf of Guinea. Atmos Environ 34:1273–1279

Almeida SM, Pio CA, Freitas MC, Reis MA, Trancoso MA (2006) Apportionment of atmospheric urban aerosol based on weekdays/weekend variability: evaluation of road re-suspended dust contribution. Atmos Environ 40:2058–2067

Amato F, Viana M, Richard A, Furger M, Prévôt ASH, Nava S, Lucarelli F, Bukowiecki N, Alastuey A, Reche C, Moreno T, Pandolfi M, Pey J, Querol X (2011) Size and time-resolved roadside enrichment of atmospheric particulate pollutants. Atmos Chem Phys 11:2917–2931

Anuforom AC (2007) Spatial distribution and temporal variability of Harmattan dust haze in sub-Sahel West Africa. Atmos Environ 41:9079–9090

Apeagyei E, Bank MS, Spengler JD (2011) Distribution of heavy metals in road dust along an urban-rural gradient in Massachusetts. Atmos Environ 45:2310–2323

Arditsoglou A, Samara C (2005) Levels of total suspended particulate matter and major aerosol at urban and semi-urban areas in Bangladesh. Atmos Environ 38:3025–3038

Assamoi EM, Liousse C (2010) A new inventory for two-wheel vehicle emissions in West Africa for 2002. Atmos Environ 44:3869–3996

Astitha M, Kallos G, Katsafados P (2008) Air pollution modeling in the 573 Mediterranean region: analysis and forecasting of episodes. Atmos Res 89:358–364

Asubiojo OI, Obioh IB, Oluyemi EA, Oluwole A, Spyrou NM, Farooqi AS, Arshed W, Akanle OA (1993) Elemental characterization of airborne particulates at two Nigerian locations during the harmattan season. J Radioanal Nucl Chem Artic 167:283–293

Athanasopoulou E, Protonotariou A, Papangelis G, Tombrou M, Mihalopoulos N, Gerasopoulos E (2016) Long-range transport of Saharan dust and chemical transformations over the Eastern Mediterranean. Atmos Environ 140:592–604

Begum BA, Kim E, Biswas SK, Hopke PK (2004) Investigation of sources of atmospheric aerosol at urban and semi-urban areas in Bangladesh. Atmos Environ 38:3025–3038

Bollati V, Marinelli B, Apostoli P, Bonzini M, Nordio F, Hoxha M, Pegoraro V, Motta V, Tarantini L, Cantone L, Schwartz J, Bertazzi PA, Baccarelli A (2010) Exposure to metal-rich particulate matter modifies the expression of candidate microRNAs in peripheral blood leukocytes. Environ Health Perspect 118:763–768

Brauer M, Hoek G, Van Vliet P, Meliefste K, Fischer P, Wijga A, Koopman L, Neijiens H, Gerritsen J, Kerkhof M, Heinrich J, Bellander T, Brunekreef B (2002) Air pollution from traffic and the development of respiratory infections and asthmatic and allergic symptoms in children. Am J Respir Crit Care Med 166:1092–1098

Caseiro A, Bauer H, Schmidl C, Pio CA, Puxbaum H (2009) Wood burning impact on PM10 in three Austrian regions. Atmos Environ 43:2186–2195

Çevik F, Göksu MZL, Derici OB, Fındık O (2009) An assessment of metal pollution in surface sediments of Seyhan dam by using enrichment factor, geoaccumulation index and statistical analyses. Environ Monit Assess 152:309–317

Chiapello I (2014) Dust observations and climatology, in mineral dust: a key player in the earth system, Dordrecht

Contini D, Cesari D, Donateo A, Chirizzi D, Belosi F (2014) Characterization of 632 PM10 and PM2.5 and their metals content in different typologies of sites in south-eastern 633 Italy. Atmosphere 5:435–453

Crawford J, Chambers S, Cohen DD, Dyer L, Wang T, Zahorowski W (2007) Receptor modelling using positive matrix factorization, back trajectories and Radon-222. Atmos Environ 41:6823–6837

D'Almeida GA (1989) A model for Saharan dust transport. J Clim Appl Meteorol 25:903–916

De Longueville F, Hountondji Y, Henry S, Ozer P (2010) What do we know about effects of desert dust on air quality and human health in West Africa compared to other regions. Sci Total Environ 409:1–8

Dimitriou K, Kassomenos P (2018) Day by day evolution of a vigorous two wave Saharan dust storm – thermal and air quality impacts. Atmosfera 31:105–124

Dongarra G, Manno E, Varrica D (2009) Possible markers of traffic-related emissions. Environ Monit Assess 154:117–125

Draxler RR, Rolph GD (2003) HYSPLIT (HYbrid Single Particle Lagrangian Integrated Trajectory) model. NOAA Air Resources Laboratory, Silver Spring

Engelstaedter S, Tegen I, Washington R (2006) North African dust emissions and transport. Earth Sci Rev 79:73–100

Ette AII (1971) The effect of the Harmattan dust on atmospheric electric parameters. J Atmos Terr Phys 33:295–300

Ezeh GC, Ugwo JP, Adebiyi FM, Abiye OE, Onwudiegwu CA, Obiajunwa EI (2018) Proton-induced X-ray emission (PIXE) analysis of trace elements of total atmospheric deposit (TAD) around a smelting industry: aerial pollution monitor. Hum Ecol Risk Assess 24:925–940

Falaiye OA, Aweda FO (2018) Trace metals and mineral composition of harmattan dust haze in Ilorin city, Kwara state, Nigeria. J Appl Sci Environ Manag 22:281–285

Falaiye OA, Yakubu AT, Aweda FO, Abimbola OJ (2013) Mineralogical characteristics of harmattan dust in Ilorin, Sub-Sahara Africa. IFE J Sci 15:175–181

Fawole OG, Olofinjana B, Owoade OK (2016) Compositional and air-mass trajectory analysis of a heavy dust episode (HDE) aerosols in Ile-Ife, Nigeria. Br J Appl Sci Technol 13:1–15

Gao Y, Nelson DE, Field PM, Ding Q, Li H, Sherrel MR, Gigliotti LC, Van Ry AD, Glenn RT, Eisenveich JS (2002) Characterization of atmospheric trace elements on PM2.5 particulate matter over the New York—New Jersey harbor estuary. Atmos Environ 36:1077–1086

Gonzalez-Martin C, Teigell-Perez N, Valladares B, Griffin DW (2014) The global dispersion of pathogenic microorganisms by dust storms and its relevance to agriculture. Adv Agron 127:1–41

Greilinger M, Zbiral J, Kasper-Giebl A (2019) Desert dust contribution to PM10 loads in Styria (Southern Austria) and impact on exceedance of limit values from 2013–2018. Appl Sci 9:2265. https://doi.org/10.3390/app9112265

Gutknecht W, Flanagan J, McWilliams A, Jayanty RKM, Kellogg R, Rice J, Duda P, Sarver RH (2010) Harmonization of uncertainties of X-ray fluorescence data for PM2.5 air filter analysis. J Air Waste Manage Assoc 60:184–194

Harrison RM, Jones AM, Gietl J, Yin J, Green DC (2012) Estimation of the contributions of brake dust, tire wear, and resuspension to nonexhaust traffic particles derived from atmospheric measurements. Environ Sci Technol 46:6523–6529

Kallos G, Astitha M, Katsafados P, Spyrou C (2007) Long-range transport of anthropogenically and naturally produced particulate matter in the Mediterranean and North Atlantic: current state of knowledge. J Appl Meteorol Climatol 46:1230–1251

Knippertz P, Fink AH, Deroubaix A, Morris E, Tocquer F, Evans MJ, Flamant C, Gaetani M, Lavaysse C, Mari C, Marsham JH, Meynadier R, Affo-Dogo A, Bahaga T, Brosse F, Deetz K, Guebsi R, Latifou I, Maranan M, Rosenberg PD, Schlueter A (2017) A meteorological and chemical overview of the DACCIWA field campaign in West Africa in June–July 2016. Atmos Chem Phys Discuss. https://doi.org/10.5194/acp-2017-345

Kothai P, Saradhi IV, Pandit GG, Puranik VD (2011) Chemical characterization and source identification of PM at urban site of Mumbai India. Aerosol Air Qual Res 11:560–569

Liousse C, Assamoi E, Criqui P, Granier C, Rosset R (2014) African combustion emission explosive growth from 2005 to 2030. Environ Res Lett. https://doi.org/10.1088/1748e9326/9/3/035003

Manousakas M, Diapouli E, Papaefthymiou H, Kantarelou V, Zarkadas C, Kalogridis A-C, Karydas A-G, Eleftheriadis K (2017) XRF characterization and source apportionment of PM10 samples collected in a coastal city. X-Ray Spectrom 1–11

Mari CH, Reeves CC, Law KS, Ancellet G, Andres-Hernandez MD, Barret B, Bechara J, Borbon A, Bouarar I, Cairo F, Commane R, Delon C, Evans MJ, Fierli F, Floquet C, Galy-Lacaux C, Heard DE, Homan CD, Ingham T, Larsen N, Lewis AC, Liousse C, Murphy JG, Orlandi E, Oram DE, Saunois M, Serca D, Stewart DJ, Stone D, Thouret V, van Velthoven P, Williams JE (2011) Atmospheric composition of West Africa: highlights from the AMMA international program. Atmos Sci Lett 12:13–18

Mason B, Moore BC (1982) Principles of geochemistry, New York

Masri S, Garshick E, Hart J, Bouhamra W, Koutrakis P (2017) Use of visual range measurements to predict fine particulate matter exposures in southwest Asia and Afghanistan. J Air Waste Manage Assoc 67:75–85

McTainsh GH, Nickling WG, Lynch AW (1997) Dust deposition and particle size in Mali, West Africa. Catena 29:307–322

Nastos PT, Bleta AG, Matsangouras IT (2016) Human thermal perception related to Föhn winds due to Saharan dust outbreaks in Crete Island, Greece. Theor Appl Climatol 1–13. https://doi.org/10.1007/s00704-015-1724-3

Ogungbenro SB, Morakinyo TE (2014) Rainfall distribution and change detection across climatic zones in Nigeria. Weather Clim Extremes 5:1–6

Omotosho JB, Abiodun BJ (2007) A numerical study of moisture build-up and rainfall over West Africa. Meteorol Appl 14:209–225

Pant P, Harrison RM (2013) Estimation of the contribution of road traffic emissions to particulate matter concentrations from field measurements: a review. Atmos Environ 77:78–97

Peltier RE, Cromar KR, Ma Y, Fan Z-H, Lippmann M (2011) Spatial and seasonal distribution of aerosol chemical components in New York City: (2) road dust and other tracers of traffic-generated air pollution. J Expo Sci Environ Epidemiol 21:484–494

Polymenakou PN, Mandalakis M, Stephanou EG, Tselepides A (2008) Particle size distribution of airborne microorganisms and pathogens during an intense African dust event in the eastern Mediterranean. Environ Health Perspect 116:292–296

Prospero JM, Ginoux P, Torres O, Nicholson SE, Gill TE (2002) Environmental characterization of global sources of atmospheric soil dust identified with the nimbus 7 total ozone mapping spectrometer (TOMS) absorbing aerosol product. Rev Geophys 40:1002. https://doi.org/10.1029/2000RG000095

Qin Y, Chan KC, Chan YL (1997) Characteristics of chemical compositions of atmospheric aerosols in HongKong: spatial and seasonal distributions. Sci Total Environ 206:25–37

Reimann C, Caritat P (2000) Enrichment factors (EFs) in environmental geochemistry. Environ Sci Technol 34:5084–5091

Resch F, Sunnu A, Afeti G (2008) Saharan dust flux and deposition rate near the Gulf of Guinea. Chem Phys Meteorol 60:98–105

Rissler J, Swietlicki E, Bengtsson A, Boman C, Pagels J, Sandstrom T, Blomberg A, Londahl J (2012) Experimental determination of deposition of diesel exhaust particles in the human respiratory tract. J Aerosol Sci 48:18–33

Rodriguez S, Querol X, Alastuey A, Kallos G, Kakaliagou O (2001) Saharan dust contributions to PM10 and TSP levels in Southern and Eastern Spain. Atmos Environ 35:2433–2447

Rolph G, Stein A, Stunder B (2017) Real-time environmental applications and display sYstem: READY. Environ Model Softw 95:210–228

Shao Y, Wyrwoll KH, Chappell A, Huang J, Lin Z, McTainsh GH, Mikami M, Tanaka TY, Wang X, Yoon S (2011) Dust cycle: an emerging core theme in earth system science. Aeolian Res 2:181–204

Song F, Gao Y (2011) Size distributions of trace elements associated with ambient particular matter in the affinity of a major highway in the New Jersey New York metropolitan area. Atmos Environ 45:6714–6723

Stein AF, Draxler RR, Rolph GD, Stunder BJB, Cohen MD, Ngan F (2015) NOAA's HYSPLIT atmospheric transport and dispersion modeling system. Bull Am Meteorol Soc 96:2059–2077

Sunnu A, Afeti G, Resch F (2008) A long-term experimental study of the Saharan dust presencein West Africa. Atmos Res 87:13–26

Tanaka TY, Chiba MA (2006) Numerical study of the contribution of dust source regions to the global dust budget. Glob Planet Chang 52:88–104

Wahlin P, Berkowicz R, Palmgren F (2006) Characterization of traffic-generated particulate matter in Copenhagen. Atmos Environ 40:2151–2159

Watson GJ, Chow CJ, Houck JE (2001) PM2.5 chemical source profiles for vehicle exhaust, vegetative burning, geological material and coal burning in Northwestern Colorado during 1995. Chemosphere 43:1141–1151

WHO (2006) Air quality guidelines for particulate matter, ozone, nitrogen dioxide and sulfur dioxide, Global update 2005. World Health Organization, Geneva

WHO (2016) Ambient (Outdoor) air quality and health. http://www.who.int/mediacentre/factsheets/fs313/en/